Open Ceramics 5 (2021) 100075

Contents lists available at ScienceDirect

Open Ceramics

journal homepage: www.editorialmanager.com/oceram

Flash spark plasma sintering of pure TiB_2

Simone Failla [a,*], Shuai Fu [b], Diletta Sciti [a], Salvatore Grasso [b,**]

[a] CNR-ISTEC, National Research Council of Italy - Institute of Science and Technology for Ceramics, Via Granarolo 64, 48018, Faenza, Italy
[b] Key Laboratory of Advanced Technologies of Materials, Ministry of Education, School of Materials Science and Engineering, Southwest Jiaotong University, Chengdu 610031, China

ARTICLE INFO

Keywords:
Spark plasma sintering
Flash sintering
Ultra high temperature ceramics

ABSTRACT

Flash Spark Plasma Sintering (FSPS) was used to rapidly sinter pure titanium diboride (TiB_2). A pre-sintered sample (Ø = 20 mm with relative density 60%) was crossed under a current of 2–2.5 kA flowing entirely across the sample. The samples were locally densified up to 98% of relative density in a very short time of 20 s. The rapid heating (≈6000 °C/min) prevented the complete evaporation of B_2O_3, leading to the formation of rarely seen segregation of boron at the grain boundaries. Compared to SPS or hot press, the rapid FSPS processing promoted the formation boron rich grain boundaries during sintering, thus enhancing consolidation. The FSPS approach might be suitable to consolidate other refractory borides.

1. Introduction

Chemical-physical properties of ceramics are closely dependent on their microstructural evolution experienced during sintering. The precise control over microstructural design has driven technological advances in the consolidation techniques [1]. In the recent years, this has resulted in innovative sintering techniques which have surpassed traditional pressureless sintering (PLS) in terms of energy efficiency, production costs and performance of the final products. Difficult to consolidate structural ceramics (i.e., SiC, Si_3N_4, TiN, WC, TiB_2, HfC etc.) typically require the application of an external pressure to obtain dense bulks while suppressing detrimental grain growth. Hot pressing (HP) or hot isostatic pressing (HIP) have enabled the consolidation of refractory compounds while reducing their processing temperatures. Starting from the nineties, Spark Plasma Sintering (SPS), activated by the flow of a pulsed electric current, has contributed to further promote densification rates while reducing processing times. Consolidation methods based on an electrical discharge can even been further speeded up by localizing the heat on the sintering sample [2]. As a reference processing timescale, a hot press cycle of TiB_2 requires several hours, an SPS cycle 1 h, while flash-SPS (FSPS) less than a minute.

The first flash sintering (FS) experiments were conducted by Cologna et al. [3], on zirconia and full densification was achieved at the furnace temperature of 850 °C under a discharge of a few hundred milliamperes for 5 s. Since then, this technique has attracted a lot of attention from material scientists because it offers great energy savings and a drastic reduction in process times. Recent studies conducted by Grasso et al. [4] have shown that it is possible to modify the SPS technique to achieve the so called "flash" sintering, also known as FSPS event using commercially available SPS units. FSPS employs Joule heating generated by the passage of an electric current (≈kA) across the conductive ceramics (i.e., ZrB_2, HfB_2). High sintering temperatures up to 2000–2500 °C are achieved contributing to rapid densification in extremely short time (10–60 s) [5].

FSPS combines the advantages of FS and SPS. It replaces the FS platinum electrode with an inexpensive graphite one, it allows the production of large samples (Ø ≈10 cm) diameter using a low voltage (<10 V). So far, FSPS has confirmed that is possible to attain high densities in a very short time (<1 min) for different systems including ZrB_2 [4], HfB_2 [6], SiC [7,8], B_4C [9], ZrO_2 [10], TiB_2-hBN [11]. Finite Element Method (FEM) was found particularly useful to predict/reduce thermal gradients within the sintering samples and shorten the processing times. Some studies [7,12,13] confirmed an increased sintering efficiency for "die-less" configuration as it allows to concentrate the current flow on the sample. The absence of a graphite die might allow a smooth transition to automated sintering systems based on a rotary table.

TiB_2 is an ultra-high temperature ceramic material (UHTC) with a unique combination of physical and structural characteristics such as high hardness (25–30 GPa), high modulus and high strength (560 GPa) retained up to elevated temperature, and a melting point $T_m = 3225$ °C [14]. Similar to metals, TiB_2 bulks have a good electrical conductivity

* Corresponding author.
** Corresponding author.
E-mail addresses: simone.failla@istec.cnr.it (S. Failla), s.grasso@swjtu.edu.cn (S. Grasso).

https://doi.org/10.1016/j.oceram.2021.100075
Received 9 December 2020; Received in revised form 4 February 2021; Accepted 8 February 2021

that allows machining using electro discharge machining (EDM). The presence of an undesirable oxide layer on the surface of TiB_2 powder particles hinders its densification [15,16]. Surface oxides are in the form of TiO_2 and B_2O_3, so, high temperatures and prolonged sintering times are required to achieve densities exceeding 90%. The SPS literature on pure TiB_2 indicates as typical processing parameters a dwelling time of 20–30 min at 1500–1900 °C with heating rate of 150 °C/min under a 40–70 MPa of mechanical pressure [17–20].

In this work, the feasibility of FSPS applied to TiB_2 has been investigated for first time. Microstructural analyses were carried out using a scanning electron microscope and X-Ray diffraction to observe the microstructural and structural modifications induced by the extremely rapid FSPS heating rates.

2. Materials and methods

2.1. Pre-sintering

Commercial powders of titanium diboride, TiB_2 (H.C. Starck, Grade F, D_{90} 4.0–7.0 μm, D_{50} 2.5–3.5 μm, $\rho = 4.52$ g/cm^3, impurities (wt. %): 0.4C, 2.5 O, 0.5 N, 0.1 Fe), were used to produce pellets with $Ø = 20$ mm, as listed in Table 1. TiB_2 pellets were pre-sintered using a spark plasma sintering furnace (Chenhua 10–20 SPS furnace, China), at 1600 °C in low vacuum (5 Pa) under uniaxial mechanical pressure of 25 MPa, heating rate of 80 °C/min and dwelling time of 10 min. This step resulted in limited densification and allowed to remove the oxide impurities from the as received powders. After pre-sintering, the densities were calculated from geometrical parameters and the relative density was in the range 50–60%. At this stage the TiB_2 disks were strong enough (i.e. hold the contact pressure of the SPS machine) to be processed using the FSPS method. FSPS configuration, shown in Fig. 1, is die-less and the current was entirely concentrated across the sample.

2.2. Sintering

Each sample was surrounded on top, bottom and sidewise by a soft graphite felt, as shown in Fig. 1, with the purpose of thermally insulating the sample and preventing the sample cracking during the heating and cooling ramp. The die-less configuration did not allow to measure the real temperature during the thermal cycle because the side pyrometer was focused on the felt itself. Due to the difficulties in measuring the actual sample temperature, the electric power was cut off when the displacement of the rams reached a predetermined value of ≈2 mm, which according to our calculations corresponded to a relative density exceeding 90%. A constant uniaxial pressure of 25 MPa was maintained during FSPS. Experiments were carried by using a voltage of 7 and 9 V in order to account for the heating power on densification. The current raise rate was around 100 A/s meaning that after 10 s the current reached ≈1000 A. Bulk densities were measured by the Archimedes' method. Since the external areas of the samples were porous, the work was focused on the microstructural analysis of the full dense central areas (radius ≈6.5 mm) of the materials. In this work the potentials of FSPS were explored. A further optimization of the die setups could have improved the homogeneity of the samples as proposed in Ref. [11].

2.3. Characterization

The microstructure was analyzed on polished cross sections, using diamond discs up to 0.25 μm, by field-emission scanning electron microscopy (FESEM, mod. ΣIGMA, ZEISS NTS Gmbh, Oberkochen, Germany) equipped with energy X-ray dispersive microanalysis (EDS, Model INCA energy 300; Oxford Instruments, UK). Image analysis (Image-Pro Plus® version 7, Media Cybernetics, Silver Springs, MD, USA) of FESEM micrographs was used to measure the mean grain size and the residual porosity of the dense central area of the sintered samples. Crystalline phases of the samples were identified by X-ray diffraction (XRD, mod. D8 Advance - Bruker, Germany) with Cu Kα radiation, step size of 0.04 and 0.5 s counting rate in the 20–80° 2θ range.

3. Results and discussion

The densities determined using the Archimedes method, processing conditions and grain size of the Flash-SPS TiB_2 are summarized in Table 1. These samples were processed under a FSPS voltage of 7 and 9 V for 40 and 20 s respectively. Despite the different conditions, the final bulk relative densities were 87% for both samples. The relevant processing were current ~2–2.4 kA, electrical resistance of 3.5–5 mΩ, and heating power of 15–22 kW. The pressure was maintained at 25 MPa to avoid crack formation during the forging/sintering process.

3.1. Microstructure

According to the X-ray diffraction pattern for TB1 and TB2 samples, Fig. 2, only TiB_2 reflections were detected. No undesirable phases, such as TiB, were observed, as were instead detected in conventional SPS-ed materials [18]. [21]. The diffraction pattern of commercial powder and reference pattern are shown in Fig. 2 for comparison. XRD patterns refer to the surfaces normal to the SPS pressing direction for both samples. The intensities reflections for both sintering samples were not in accordance with the reference diffraction pattern (TiB_2: JCPDF card 35–0741). A preferential orientation of the (001) and (002) planes along the FSPS direction was observed (Fig. 2) in accordance with the work of Jensen et al. [22].

Details of the microstructure can be observed in Fig. 3. Focusing our attention on the dense area of the materials, porosity was detected inside the grains, Fig. 3c, and at the grain boundaries. Comparing the two samples, a further increase in relative power of SPS furnace resulted in no significant change in the overall density, but the microstructures presented some relevant differences. Sample TB1, sintered with 7 V and 40 s, presented areas with very high density, exceeding 98% and with an average grain size of 14.4 μm. On the contrary, sample TB2, sintered under the peak power of 22 kW for just 20 s, featured finer grains of 9.5 μm associated with a significant phase segregation at the grain boundaries, arrows and inset in Fig. 3f, as discussed below.

Due to a low self-diffusion coefficient, strong covalent bonding and high vapor pressure, it is difficult to consolidate borides such as ZrB_2, TiB_2 or HfB_2 up to a density exceeding 90–95% with conventional sintering methods (HP, SPS, PLS). Turan et al. [19] examined different sintering parameters of monolithic TiB_2 with SPS method. By analyzing

Table 1
FSPS configuration, sintering time, mean grain size (m.g.s.), density and relative density of the FSPS samples.

Sample	Pressure	Relative power of SPS	Max current	Voltage	Power[a]	Discharge Time	m.g.s dense area (Center)	m.g.s porous area (Rim)	Bulk Density[b]	Local relative density (SEM)[c]
	MPa	%	kA	V	kW	sec	μm	μm	g/cm^3	%
TB1	25	70	2	7	15	40	14.4 ± 6.9	5.9 ± 2	3.9	98.1
TB2		90	2.4	9	22	20	9.5 ± 4.1	5.3 ± 1.5	3.9	98.3

[a] Peak power.
[b] Bulk density measured using Archimedes 'method was 87% of relative density for both samples.
[c] Relative densities of the central areas of the materials measured using image analysis software.

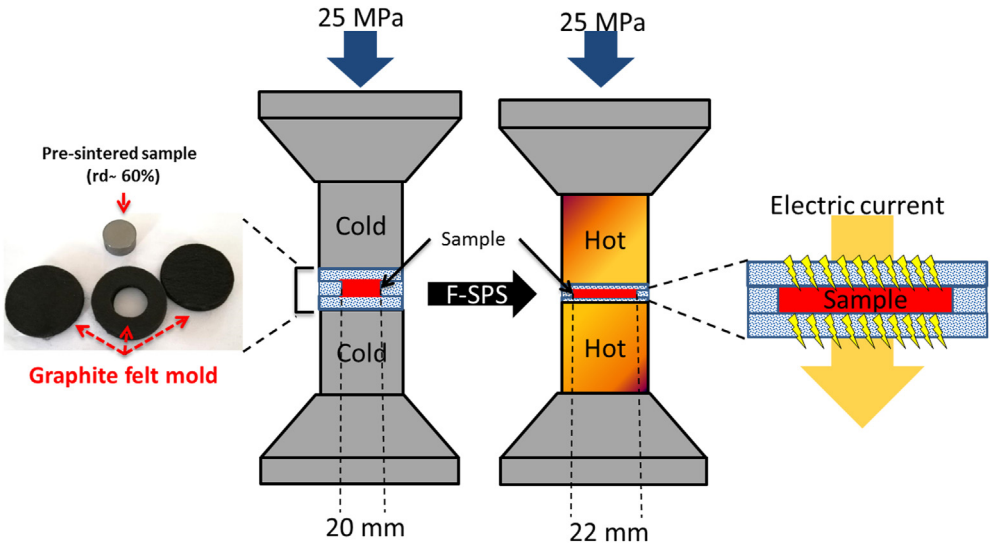

Fig. 1. Schematic of the Flash-SPS die-less configuration.

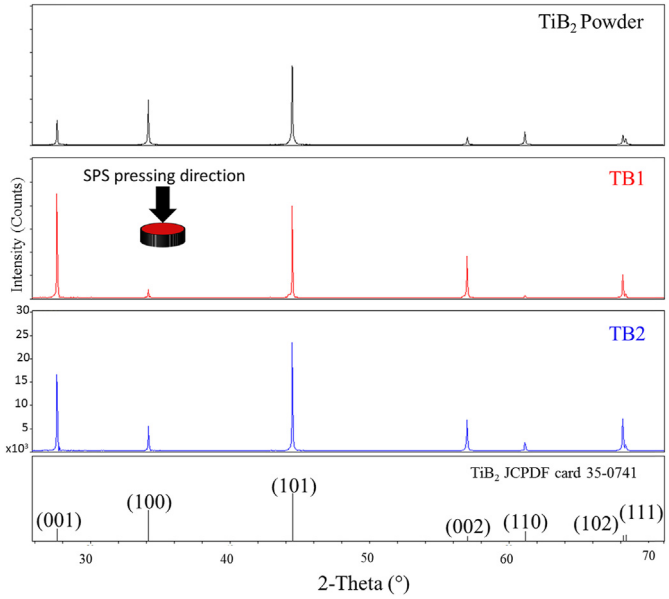

Fig. 2. XRD patterns showing the only TiB_2 phase in TB1 and TB2 samples.

the effects of temperature and pressure application schedule, they were unable to obtain relative densities higher than 80% due to the presence of oxides (e.g. B_2O_3, TiO_2 for TiB_2) [15]. [16]. Similarly, Tatarko et al. [23] using the same grade powders of this study achieved a density of 85% with a grain size of ≈10 μm after SPS 2100 °C under an external pressure of 90 MPa.

The removal of the oxide coating from the particles surface plays a very important role on the densification mechanisms of titanium diboride. As the densification advances, gases deriving from reduction/sublimation of oxides remain trapped in the pores, preventing their closure. As a consequence, the densification slows down and grain growth is favored. In TiB_2, grain growth can result in the formation of entrapped intragranular porosity above 90% of relative density. In the materials of the present work, pores in TB1 were clearly spherical inside the grains. On the other side, TB2 porosity had an irregular shape and contained unreacted phases [24,25].

To elucidate the possible FSPS sintering mechanism, we considered a comparison with other sintering techniques. In conventional sintering the slow heating (≈10 °C/min) allows removal of gas phases at low temperature (1000–1500 °C), before closed porosity appears [16,26]. The FSPS heating rate above 6000 °C/min could be high enough to shift the evaporation temperature upward hindering the complete elimination of spurious phases. Surprisingly, FSPSed samples showed no traces of oxygen, but revealed an intergranular phase mainly containing boron and carbon, Fig. 3g)–i). This phase was not observed in materials processed using SPS [19–21] or hot pressing [27]. A possible explanation for such difference could be attributed to the equilibrium vapor pressure of liquid B_2O_3 and its gas, shown in figure in Fig. 4 [16,28]. Under slow heating (≈100 °C/min for SPS), in the temperature range of 1200 and 1400 °C, the vapor pressure of molten B_2O_3 reaches the furnace environment pressure and it might vaporize completely, accordingly to (1):

$$B_2O_3\ (l) \rightarrow B_2O_3\ (g) \quad (1)$$

Experimentally, Huang et al. [29] determined that during sintering of TiB_2 composites, the vacuum pressure increased significantly at 1750 °C confirming the sublimation of boron oxide. The as-received TiB_2 contained 2.5 wt% of oxygen impurities. As previously mentioned, dark contrasting phases were recognized in all the samples along the grain boundaries, see Fig. 3g)–i). According to SEM-EDS analyses the dark phases were B and C-based phases. Presence of carbon is not surprising and it is attributed to free carbon from the starting powder that did not have sufficient time to react. Formation of Boron was not observed in other works [17–20] and it may be ascribed to the following reaction.

$$B_2O_3\ (l) + C \rightarrow 2B + 3CO\ (g) \quad (2)$$

Due to fast FSPS heating, the free carbon reacted with the boron oxide before the latter was converted into a vapor phase. The diagram in Fig. 4 shows that in equilibrium conditions the presence of carbon favours the formation of CO gas at temperatures below 1000 °C. B_2O_3 has enough time to evaporate in conventional SPS or hot press. On the contrary, the extremely short FSPS cycle, lasting only 20 or 40 s, did not allow B_2O_3 sublimation and formation of boron was instead promoted. Looking at Fig. 3g and h, boron appears as a liquid phase between the grains, which explains the ultrafast sintering rates observed. The presence of molten boron suggests the sintering temperature exceeded 2080 °C [30] and the liquid phase accelerated the densification because it reduced the activation energy for sintering at the expenses of a rapid grain growth (grains grew up to 14 μm within 40 s). A more complete understanding of the sintering mechanism might require further investigation as the electrical conductivity of the boron-rich phase is a two order of magnitude lower than TiB_2 resulting in a differential heating, as modelled by Wu et al.

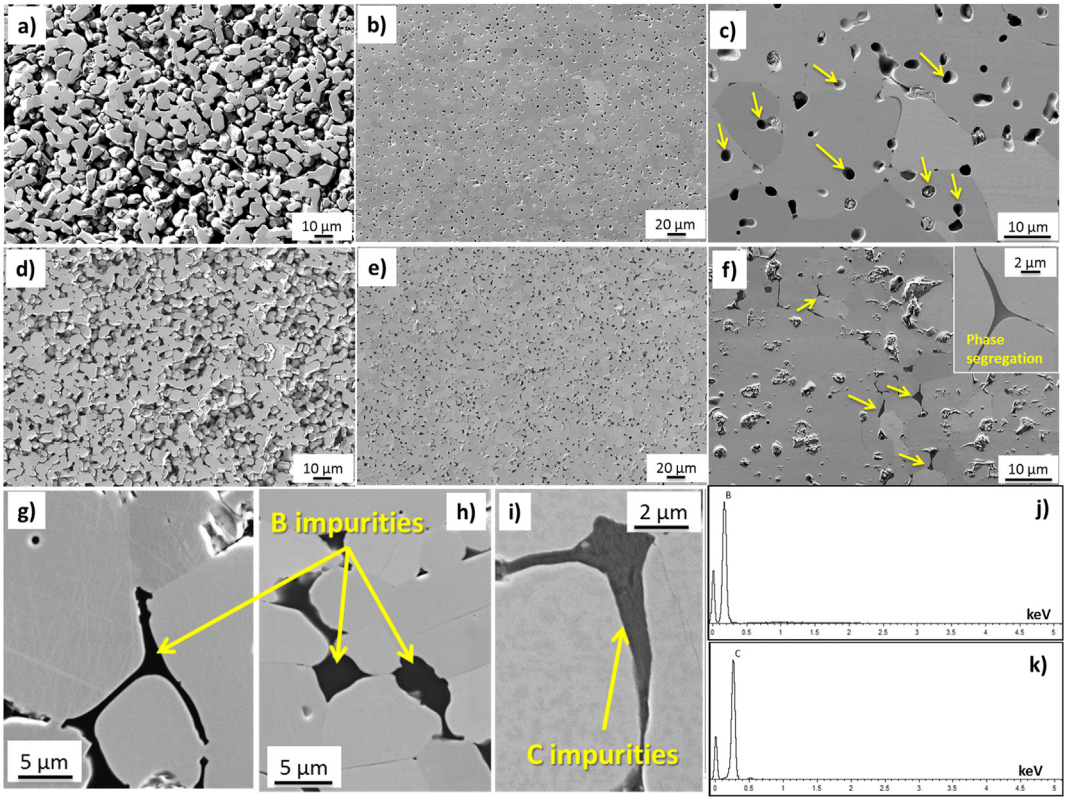

Fig. 3. SEM images showing the microstructure of material TB1 (a–c, g, h) and TB2 (d–f, i): a), d) less dense areas; b), e) high density areas; c) the arrows point porosities inside the grains of high density areas and f) phase segregation. EDS spectra (j–k) of dark phases segregations present in both materials (g–i).

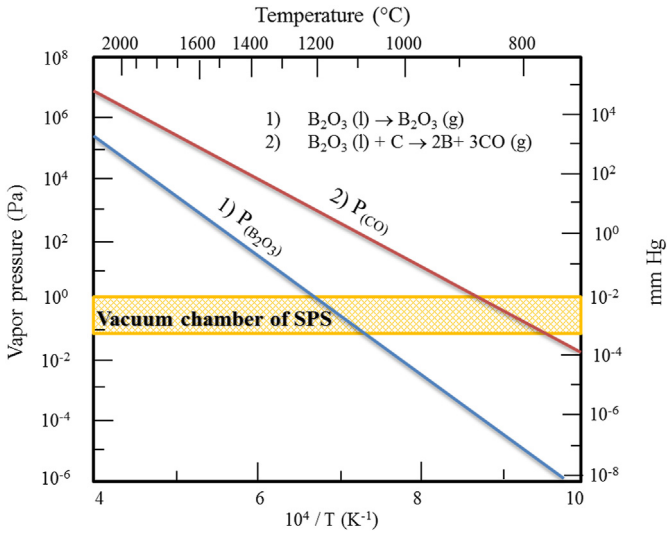

Fig. 4. Equilibrium vapor pressure of B_2O_3 and CO gases as function of temperature [16]. The representation is indicative for reactions occurring at different heating rates: Reaction 1) is kinetically favored in the case of SPS (heating rate 100 °C/min), while reaction 2) might be dominant in the case of FSPS (heating rate 6000 °C/min).

[13]. A comparison of the FSPSed samples with or without thermal annealing (≈2000 °C) could clearly pin down the microstructural metastability induced by the rapid processing.

4. Conclusions

Pure TiB_2 was pre-sintered using conventional SPS and subsequently consolidated by Flash Spark Plasma Sintering in a die-less configuration within 20 or 40 s, resulting in a relative density up to 98.3% in the central areas of the specimen (while its rim was less dense). The B_2O_3 oxygen impurities in the starting powders, which usually hinder sintering mechanism, seem to play a role in fast heating condition as they promoted the formation of a boron rich liquid phase which accelerated consolidation at the expenses of a fast grain growth. The rapid heating rate of FSPS (up to 6000 °C/min) confirmed the possibility to consolidate TiB_2 ceramics in short time and with remarkably reduced energy input. Compared to SPS, the accelerated FSPS heating rate seems to enhance densification of TiB_2 because of the formation of a thermodynamically metastable boron based liquid phase.

Declaration of competing interest

The authors declare that they have no known competing financial interests or personal relationships that could have appeared to influence the work reported in this paper.

Acknowledgments

SG was supported by Thousand Talents Program of China and Sichuan Province.

References

[1] M. Biesuz, S. Grasso, V.M. Sglavo, What's new in ceramics sintering? A short report on the latest trends and future prospects, Curr. Opin. Solid State Mater. Sci. 24 (2020) 100868, https://doi.org/10.1016/j.cossms.2020.100868.
[2] C. Wang, W. Ping, Q. Bai, H. Cui, R. Hensleigh, R. Wang, A.H. Brozena, Z. Xu, J. Dai, Y. Pei, C. Zheng, G. Pastel, J. Gao, X. Wang, H. Wang, J.C. Zhao, B. Yang, X. Zheng, J. Luo, Y. Mo, B. Dunn, L. Hu, A general method to synthesize and sinter bulk ceramics in seconds, Science 368 (80) (2020) 521–526, https://doi.org/10.1126/science.aaz7681.
[3] M. Cologna, B. Rashkova, R. Raj, Flash sintering of nanograin zirconia in <5 s at 850°C, J. Am. Ceram. Soc. 93 (2010) 3556–3559, https://doi.org/10.1111/j.1551-2916.2010.04089.x.

[4] S. Grasso, T. Saunders, H. Porwal, O. Cedillos-Barraza, D.D. Jayaseelan, W.E. Lee, M.J. Reece, Flash spark plasma sintering (FSPS) of pure ZrB_2, J. Am. Ceram. Soc. 97 (2014) 2405–2408, https://doi.org/10.1111/jace.13109.

[5] M. Yu, S. Grasso, R. Mckinnon, T. Saunders, M.J. Reece, Review of flash sintering: materials, mechanisms and modelling, Adv. Appl. Ceram. 116 (2017) 24–60, https://doi.org/10.1080/17436753.2016.1251051.

[6] J. Zou, S. Grasso, L.F. Liu, H. Bin Ma, M. Reece, J. Binner, Flash spark plasma sintering of HfB_2 ceramics without pre-sintering, Scripta Mater. 156 (2018) 115–119, https://doi.org/10.1016/j.scriptamat.2018.07.026.

[7] S. Grasso, T. Saunders, H. Porwal, B. Milsom, A. Tudball, M. Reece, I.W. Chen, Flash spark plasma sintering (FSPS) of α and β SiC, J. Am. Ceram. Soc. 99 (2016) 1534–1543, https://doi.org/10.1111/jace.14158.

[8] E.A. Olevsky, S.M. Rolfing, A.L. Maximenko, Flash (Ultra-Rapid) spark-plasma sintering of silicon carbide, Sci. Rep. 6 (2016) 1–9, https://doi.org/10.1038/srep33408.

[9] B. Niu, F. Zhang, J. Zhang, W. Ji, W. Wang, Z. Fu, Ultra-fast densification of boron carbide by flash spark plasma sintering, Scripta Mater. 116 (2016) 127–130, https://doi.org/10.1016/j.scriptamat.2016.02.012.

[10] O. Vasylkiv, H. Borodianska, Y. Sakka, D. Demirskyi, Flash spark plasma sintering of ultrafine yttria-stabilized zirconia ceramics, Scripta Mater. 121 (2016) 32–36, https://doi.org/10.1016/j.scriptamat.2016.04.031.

[11] R. McKinnon, S. Grasso, A. Tudball, M.J. Reece, Flash spark plasma sintering of cold-Pressed TiB_2-hBN, J. Eur. Ceram. Soc. 37 (2017) 2787–2794, https://doi.org/10.1016/j.jeurceramsoc.2017.01.029.

[12] C. Manière, G. Lee, E.A. Olevsky, All-materials-inclusive flash spark plasma sintering, Sci. Rep. 7 (2017) 1–8, https://doi.org/10.1038/s41598-017-15365-x.

[13] J. Wu, B. Niu, F. Zhang, L. Lei, J. Zhang, L. Ren, W. Wang, Z. Fu, Effect of titanium diboride on the homogeneity of boron carbide ceramic by flash spark plasma sintering, Ceram. Int. 44 (2018) 15323–15330, https://doi.org/10.1016/j.ceramint.2018.05.179.

[14] B.R. Golla, T. Bhandari, A. Mukhopadhyay, B. Basu, Titanium diboride, in: W.G. Fahrenholtz, E.J. Wuchina, W.E. Lee, Y. Zhou (Eds.), Ultra-High Temp. Ceram. Mater. Extrem. Appl., 2014, pp. 316–360, https://doi.org/10.1002/9781118700853.ch13.

[15] B. Basu, G.B. Raju, A.K. Suri, Processing and properties of monolithic TiB_2 based materials, Int. Mater. Rev. 51 (2006) 352–374, https://doi.org/10.1179/174328006X102529.

[16] S. Baik, P.F. Becher, Effect of oxygen contamination on densification of TiB_2, J. Am. Ceram. Soc. 70 (1987) 527–530, https://doi.org/10.1111/j.1151-2916.1987.tb05699.x.

[17] Z.H. Zhang, X.B. Shen, F.C. Wang, S.K. Lee, L. Wang, Densification behavior and mechanical properties of the spark plasma sintered monolithic TiB_2 ceramics, Mater. Sci. Eng. 527 (2010) 5947–5951, https://doi.org/10.1016/j.msea.2010.05.086.

[18] A. Mukhopadhyay, T. Venkateswaran, B. Basu, Spark plasma sintering may lead to phase instability and inferior mechanical properties: a case study with TiB_2, Scripta Mater. 69 (2013) 159–164, https://doi.org/10.1016/j.scriptamat.2013.02.027.

[19] A. Turan, F. Cinar, G. Goller, O. Yucel, Spark plasma sintering of monolithic TiB_2 ceramics, J. Ceram. Process. Res. 15 (2014) 464–468.

[20] Ö. Balcı, U. Burkhardt, M. Schmidt, J. Hennicke, M. Barış Yağcı, M. Somer, Densification, microstructure and properties of TiB_2 ceramics fabricated by spark plasma sintering, Mater. Char. 145 (2018) 435–443, https://doi.org/10.1016/j.matchar.2018.09.010.

[21] H. Cheloui, Z. Zhang, X. Shen, F. Wang, S. Lee, Microstructure and mechanical properties of TiB-TiB_2 ceramic matrix composites fabricated by spark plasma sintering, Mater. Sci. Eng. 528 (2011) 3849–3853, https://doi.org/10.1016/j.msea.2011.01.096.

[22] M.S. Jensen, M.A. Einarsrud, T. Grande, Preferential grain orientation in hot pressed TiB_2, J. Am. Ceram. Soc. 90 (2007) 1339–1341, https://doi.org/10.1111/j.1551-2916.2007.01623.x.

[23] P. Tatarko, S. Grasso, A. Kovalčíková, D. Medveď, I. Dlouhý, M.J. Reece, Highly textured and strongly anisotropic TiB_2 ceramics prepared using magnetic field alignment (9T), J. Eur. Ceram. Soc. 40 (2020) 1111–1118, https://doi.org/10.1016/j.jeurceramsoc.2019.11.006.

[24] H. Hsueh, A.G. Evans, R.L. Coble, Microstructure development during final intermediate stage sintering I. pore-grain boundary separation, Acta Metall. 30 (1982) 1269–1279, https://doi.org/10.1016/0001-6160(82)90145-6.

[25] M.A. Spears, A.G. Evans, Microstructure development during final/intermediate stage sintering-II. Grain and pore coarsening, Acta Metall. 30 (1982) 1281–1289, https://doi.org/10.1016/0001-6160(82)90146-8.

[26] W.M. Guo, J. Vleugels, G.J. Zhang, P.L. Wang, O. Van der Biest, Effect of heating rate on densification, microstructure and strength of spark plasma sintered ZrB_2-based ceramics, Scripta Mater. 62 (2010) 802–805, https://doi.org/10.1016/j.scriptamat.2010.02.002.

[27] M.S. Jensen, M.A. Einarsrud, T. Grande, The effect of surface oxides during hot pressing of TiB_2, J. Am. Ceram. Soc. 92 (2009) 623–630, https://doi.org/10.1111/j.1551-2916.2009.02923.x.

[28] S.C. Zhang, G.E. Hilmas, W.G. Fahrenholtz, Pressureless densification of zirconium diboride with boron carbide additions, J. Am. Ceram. Soc. 89 (2006) 1544–1550, https://doi.org/10.1111/j.1551-2916.2006.00949.x.

[29] S.G. Huang, K. Vanmeensel, O.J.A. Malek, O. Van Der Biest, J. Vleugels, Microstructure and mechanical properties of pulsed electric current sintered B_4C-TiB_2 composites, Mater. Sci. Eng. 528 (2011) 1302–1309, https://doi.org/10.1016/j.msea.2010.10.022.

[30] J.L. Murray, P.K. Liao, K.E. Spear, The B-Ti (Boron-Titanium) system, Bull. Alloy Phase Diagrams 7 (1986) 550–555, https://doi.org/10.1007/BF02869864.